Towards magnetometry with nitrogen-vacancy center in diamond

Wilson Chin Yue Sum

an academic exercise presented in partial fulfillment for the degree of Bachelor of Science with Honours in Physics

Supervisor: Professor Christian Kurtsiefer

Department of Physics

National University of Singapore

2012/2013

Contents

Acknowledgement

I hereby express my greatest gratitude to my supervisor, Professor Christian Kurtsiefer for the guidance and opportunity to work on a new project related to NV center in diamond after previous year in UROPS. It has been another amazing year and wonderful experience in experimental physics.

To Gleb, I appreciate that he has allowed for greater degree of freedom to mess around after my junior year in the laboratory. He continues to be extremely patient in mentoring. I wish to thank him for the involving discussion of physics be it related to experiment or not. I would also like to express my gratitude to Alessandro for his encouragement and guidance.

My sincere thanks to Victor who has been helping me to debug various Linux problem from time to time. To Brenda, your kindness and laughter has made the project a much more relax work to do. I wish to thank Chen Ming and Peng Kian for the occasional late dinner company. To the rest of Quantum Optics group, it has been a great time to work with you.

Abstract

We aim to use nitrogen-vacancy (NV) center in diamond as quantum noise limited sensor to measure weak magnetic fields by optically detected magnetic resonance. In this thesis, we report on the setting up of a confocal microscope to observe single NV center. Diffraction limited resolution of the confocal microscope has been achieved. The spectrum of fluorescence signal which agrees with the signature spectrum of a NV center is obtained. We performed Hanbury Brown Twiss (HBT) measurement to confirm that single NV center is observed.

Chapter 1

Introduction

The capability to measure magnetic fields with high sensitivity has emerged as an important study in physics. Such study date back to 1950s when alkali vapor cells achieved record sensitivity in measurement of magnetic field.[1] Today, atomic magnetometer is known to have achieved the highest sensitivity and is widely applied in the use of magnetic resonance imaging, studies of material science and even fundamental physics research.[1, 2, 3, 4] Despite holding the current record sensitivity, ultra high sensitivity of atomic magnetometer requires it to be operated at low temperature.[1] The need for low temperature setting restricts the possibility of bringing atomic magnetometer to close proximity with a living substance, denying its capability of near field measurement to achieve higher spatial resolution.[5] Moreover, setup for high sensitivity atomic magnetometers are relatively bulky, hence imposing difficulties in miniaturizing for robust application out of laboratory.

Recent revival of interest on NV center in diamond has found its application in magnetometry. As a point defect in diamond, NV center has atomic size and ground state multiplet with long coherence time. Conveniently, the ground state multiplet can be optically readout thus allowing measurement of optically detected magnetic resonance (ODMR).[6] Moreover, photostability of NV center enables long measurement over the same center.[6] Unlike atomic system, NV center based magnetometer may retain high sensitivity even under ambient temperature because they

are intrinsically localized in the diamond matrix. Thus, it permits for realization of a simple, robust and high sensitivity magnetometer. NV center based magnetometer allows measurement at close proximity, resulting in combination of nanoscale spatial resolution and atomic scale sensitivity.[1, 7, 8] Over the past few years, pioneering work in developing NV center based system has been successfully demonstrated in using bulk diamond nanoscale imaging [9, 10, 11, 12], with the technique extended to nanodiamonds [13, 14, 15] and as well ensembles of NV centers [16, 17, 18].

To perform magnetometry, we used an efficient way to detect fluorescence from NV center. This is accomplish with a scanning confocal microscope and the details are discussed in Chapter 2. In Chapter 3, we report on the spectrum measurement of the fluorescence signal to confirm that we have observed NV center. Last, HBT (Hanbury Brown and Twiss) measurement is also performed to show that single NV center is being studied. The result is presented in Chapter 4. A brief introduction to NV centers in diamond will be presented following in this Chapter.

1.1 A brief introduction to NV center

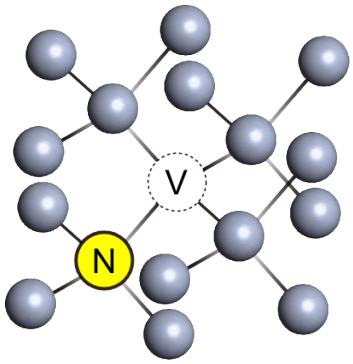

Figure 1.1: Physical structure of a NV center. A carbon atom (grey) is substituted by a nitrogen atom (N) forming a nearest neighbor pair with an adjacent lattice vacancy (V).

NV center is a defect formed by a substitutional nitrogen impurity and an adjacent lattice vacancy in diamond as shown in Figure 1.1. The determination of electronic structure of NV center has received numerous effort from theoretical research and continues so as contemporary research.[19, 20] Experimentally, it has been shown that naturally occurring NV centers exist in

form of neutral NV^0 with zero phonon line (ZPL) at 575 nm[21] and singly charged NV^- state with ZPL at 637 nm[22, 23]. In our work, we focus on NV^- state because they are dominant in natural diamond and we will refer them as NV center onwards.

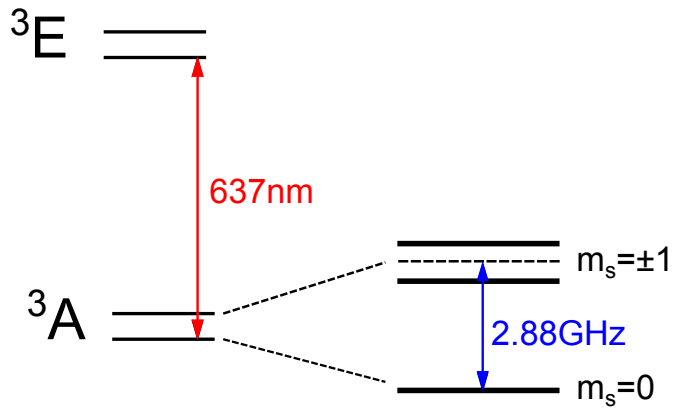

Figure 1.2: Energy level structure of a NV center. The 637 nm ZPL emission band is associated to electric dipole transition from ^{3}A to ^{3}E state. The triplet ^{3}A ground state has a zero field splitting of 2.88 GHz.

Through the combination of various theoretical and experimental work, it is determined that NV center has C_{3v} symmetry and has energy level structure as shown in Figure 1.2. The zero phonon line (ZPL) emission band of NV center at 637 nm is associated with a electric dipole transition from its ^{3}A to ^{3}E state. The presence of ^{3}A state is formed by $m_s = 0$ and two $m_s = \pm 1$ states with a zero field splitting of 2.88 GHz. Since the NV center is embedded in diamond matrix, its electronic transition ^{3}A to ^{3}E is coupled to the matrix excitation resulting in vibrationally broadened spectrum ranging from 630 nm to 750 nm.[24]

The 2.88 GHz splitting of the triplet ground electronic state and the electric dipole transition from ^{3}A to ^{3}E is used to perform optically detected magnetic resonance.[6] Amount of fluorescence from electronic transition ^{3}A to ^{3}E depends on relative occupancy of m_s states in ^{3}A multiplet. By applying a radio frequency (RF) field to the NV center, one can drive transitions between $m_s = 0$ and $m_s = \pm 1$ states. The presence of magnetic field will split the $m_s = \pm 1$ levels, driving them off resonance from the driven RF transition which will result in a change of detected fluorescence signal. That is the basic idea of optically detected magnetic resonance and how one can measure magnetic field with a NV center. To determine vector component of

the magnetic field, Ramsey-like or spin echo experiments can be performed.[7, 10]

Chapter 2

Confocal microscopy of NV center

Sensitivity of a magnetometer scales as signal strength and coherence time of the sensor, which in our case is NV center. One may use ensemble of NV centers to increase the signal strength which scales linearly with number of NV centers. However like other solid state systems, each NV center is uniquely coupled to its local environment which leads to inhomogeneous broadening that could not be easily manipulated. This broadening leads to spin dephasing that would reduce the magnetic sensitivity. Alternatively, one may work with single NV center but achieve high signal strength with efficient collection of fluorescence. For that, one may employ method of confocal microscopy.[6] In this chapter, we report on the setup of a confocal microscope to study single NV center.

2.1 Setup: Confocal microscope

We have employed technique of scanning confocal microscopy to study single NV center, with the setup shown in Figure 2.1. A 532 nm excitation laser is coupled out of a single mode fiber with an aspheric lens (f_c=11 mm). The excitation laser is focused with a microscope objective (MO) with 100x magnification and numerical aperture (NA) of 0.90 to illuminate the diamond sample (Electronic Grade Single Crystal Grade B). Using the same microscope objective, fluorescence from the diamond is extracted. The fluorescence signal is coupled into

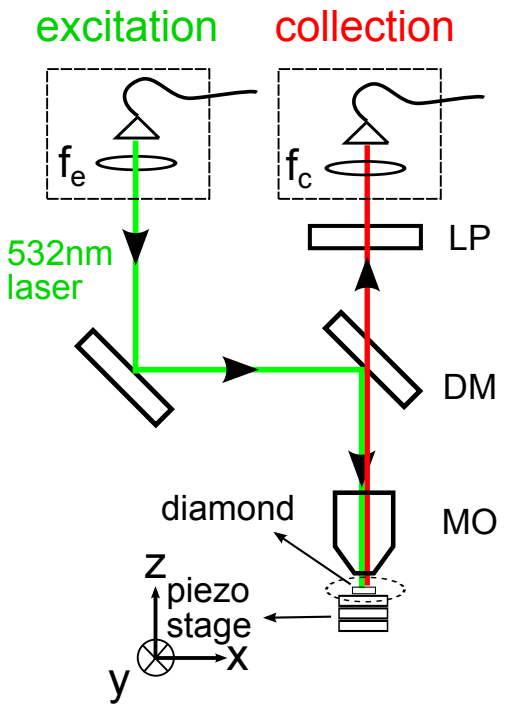

Figure 2.1: Setup schematic of the confocal microscope. An excitation laser of 532 nm is focused onto the diamond through a microscope objective (MO) and the fluorescence signal from the diamond is collected with the same MO. (f_e:aspheric lens of f=11 mm, f_c:achromatic lens of f=16.55 mm, LP:long pass filter, DM:dichroic mirror, MO:microscope objective)

another single mode fiber with an achromatic lens (f_c=16.55 mm). The achromatic lens ensures same focusing for all spectral components of the fluorescence signal. The use of single mode fiber defines a spatial mode for the excitation laser and detected signal. These modes are thus fixed to be Gaussian with properties that are discussed in details further in Section 2.1.1. A combination of long pass filter (OG590) and dichroic mirror is used to suppress scattering of the excitation laser from being collected. The fluorescence is detected by an avalanche photodetector (APD) operated in photon counting mode.

We employed a piezoelectric stage (P-611.3 NanoCube, PI) to drive the diamond sample into focus of the objective. The piezoelectric stage allows a scanning range of $120\,\mu m \times 120\,\mu m \times 120\,\mu m$ with resolution of 0.2 nm.

Selection of microscope objective (MO)

As we would be working with air to diamond interface, the difference in refractive index would result in change of collection angle defined by the MO. The collection angle is related to

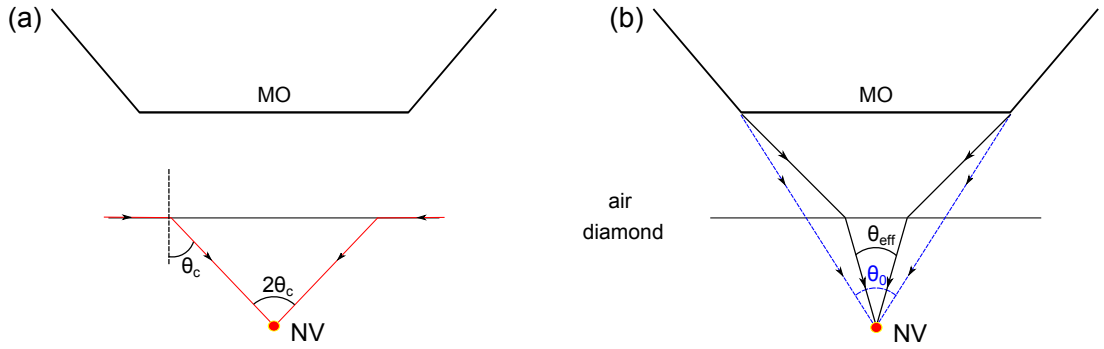

Figure 2.2: Illustration to show how focusing from air into diamond affects NA of MO. (a)Collection angle of MO is limited to $2\theta_c$ due to effect of total internal reflection. (b)Collection angle of MO is reduced from θ_0 to θ_{eff} due to effect of refraction.

numerical aperture (NA) as

$$\text{NA} = \sin\frac{\theta}{2} \tag{2.1}$$

Illustration of the effect on NA due to refraction is shown in Figure 2.2. First, total internal reflection sets maximum collection angle to critical angle of diamond resulting in NA_{max}=0.75. In addition, the MO is not designed to focus into high refractive index material. This results in reduced effective NA due to lower collection angle caused by the effect of refraction. Our choice of MO with NA=0.90 would result in estimated NA_{eff}=0.65.

2.1.1 Estimation of alignment parameters

To achieve good signal to noise ratio in detected fluorescence, it is important to overlap the excitation and collection modes on NV center. As an attempt to guide and set an upper bound for optimized alignment, the beam waist and position in the diamond with respect to misalignment of the fiber coupling lenses (f_c, f_e) is estimated.

The propagation of light through a system of optical instruments can be well described by formulation of ABCD matrix or ray transfer matrix. The concept of ABCD matrix is well established and detailed description is found in many optics textbooks.[25, 26] In our case, this concept requires to be expanded to domain of the Gaussian beams and few of the important parameters will be presented here. In this context, it is common to analyze paraxial beam

propagation in terms of the complex beam parameter or q-factor given by

$$\frac{1}{q(z)} = \frac{1}{z + iz_R} = \frac{1}{R(z)} - i\frac{\lambda}{\pi\omega^2(z)} \tag{2.2}$$

where $z_R = \pi\omega_0^2/\lambda$ is the Rayleigh range, $R(z) = z[1 + (z_R/z)^2]$ is the radius of curvature and $w_z = w_0\sqrt{1 + (z/z_R)^2}$ is the beam waist. In the analysis of ABCD matrix, the Gaussian beam can be propagated through an optical system using the equation:

$$q_2 = \frac{Aq_1 + B}{Cq_1 + D} \tag{2.3}$$

in which q_1 represents the beam before passing through the system, and q_2 describes it after the system.

ABCD matrix of our system

ABCD Matrix	Description
$\mathrm{T}_1 = \begin{pmatrix} 1 & d + f_{\text{offset}} \\ 0 & 1 \end{pmatrix}$	Translation from fiber to lens with d=$\mathrm{f}_e(\mathrm{f}_c)$
$\mathrm{F} = \begin{pmatrix} 1 & 0 \\ \frac{-1}{f_e(f_c)} & 1 \end{pmatrix}$	Fiber collimation lens with $\mathrm{f}_e(\mathrm{f}_c)$=11(16.55) mm
$\mathrm{T}_2 = \begin{pmatrix} 1 & d_2 \\ 0 & 1 \end{pmatrix}$	Translation from lens to microscope objective with d_2 =20 cm
$\mathrm{MO} = \begin{pmatrix} 1 & 0 \\ \frac{-1}{f} & 1 \end{pmatrix}$	Microscope objective with f=2mm
$\mathrm{T}_3 = \begin{pmatrix} 1 & d_3 \\ 0 & 1 \end{pmatrix}$	Translation from microscope objective to diamond surface with d_3=195 mm
$\mathrm{R} = \begin{pmatrix} 1 & 0 \\ 0 & \frac{1}{n} \end{pmatrix}$	Refraction from air into diamond with n=2.42602(2.41178)
$\mathrm{T}_4 = \begin{pmatrix} 1 & d_4 \\ 0 & 1 \end{pmatrix}$	Translation through d_4=depth in diamond matrix

We list out the ABCD matrices used to describe our system. Thin lens approximation is applied to all three lenses (f_c, f_e, MO). The system described here is shown in Figure 2.3. The initial beam parameter is given by numerical aperture (NA) of the optical fiber for 532 nm (NA=0.14)

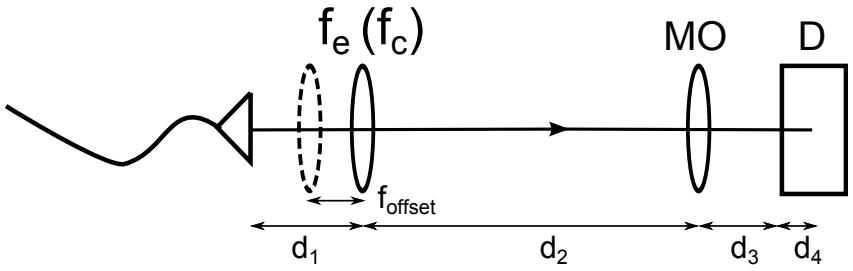

Figure 2.3: Refrence for schematic for ABCD matrix formalism of the confocal microscope. (f_e:excitation lens, f_c:collection lens, MO:microscope objective, D:diamond)

and 637 nm (NA=0.12). Hence, the ABCD matrix is given by

$$\mathrm{ABCD} = \mathrm{T}_4 \cdot \mathrm{R} \cdot \mathrm{T}_3 \cdot \mathrm{MO} \cdot \mathrm{T}_2 \cdot \mathrm{F_c} \cdot \mathrm{T}_1 \tag{2.4}$$

and can be used to predict the beam waist and position in the diamond as a function of focus offset.

Results of estimation

In this simulation of ray tracing, we use a 532 nm Gaussian beam to represent the excitation laser and 637 nm Gaussian beam to represent the fluorescence signal. The response of the waist position in depth of diamond as a function of offset of collimation lens with respect to focal position is plotted in Figure 2.5 as reference for alignment. Steep response to focus of the excitation mode shows that a slight displacement would result in misalignment with overlap of collection mode. In Figure 2.4 we show the estimated waist size in diamond with the two collimation lens placed at its respective focal position. We obtained a minimum Gaussian waist of $w_e = 0.341\,\mu$m for the excitation laser and $w_c = 0.312\,\mu$m for the fluorescence signal. For a confocal microscope, effective waist of the fluorescence signal is determined by the product of the intensity spatial profile of the excitation and collection mode. Hence, we obtain an effective waist of $w_0 = 0.326\,\mu$m.

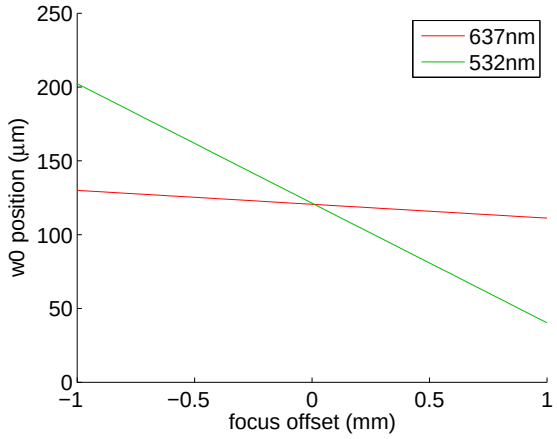

Figure 2.4: Position of waist of the 532 nm beam (excitation) and 637 nm beam (collection) in diamond as a function of focus offset.

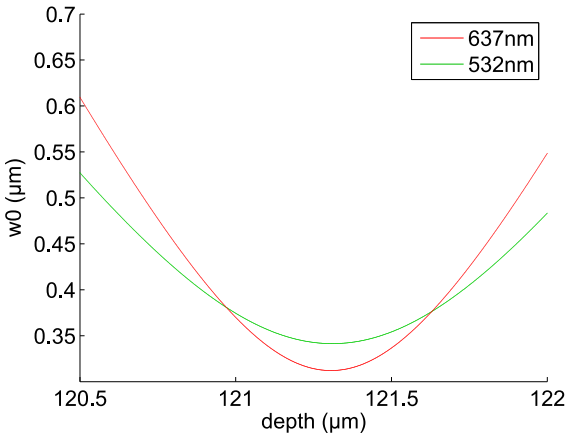

Figure 2.5: Waist size of the 532 nm beam (excitation) and 637 nm beam (collection) as a function of depth in the diamond sample.

2.2 Results

2.2.1 The search for NV center

To locate NV centers, the piezoelectric stage is scanned to drive the diamond sample across focus of the confocal microscope. We first drive the piezoelectric stage to scan into the diamond (yz plane) with a range of $90\,\mu m \times 90\,\mu m$. The fluorescence count obtained from the scan is shown in Figure 2.6. The bright band around z=20 μm displays scattering of 532 nm light off the diamond surface. This gives us position of diamond surface as a reference. Numerous number of fluorescence spots can also be observed across the diamond. We next choose a depth to perform lateral scan (xy plane) with the results shown in Figure 2.7. With the map constructed by these scans, it is possible to revert to the same fluorescence spot.

The piezoelectric stage is set to position one of the fluorescence spots to be at focus of the confocal microscope, i.e. position of maximum fluorescence intensity. We further optimize the excitation and collection optics to increase the signal strength. For a good overlap of excitation and collection mode in a confocal microscope, fluorescence from a single emitter with atomic size such as NV center should be diffraction limited. We confirm that by performing a fine lateral

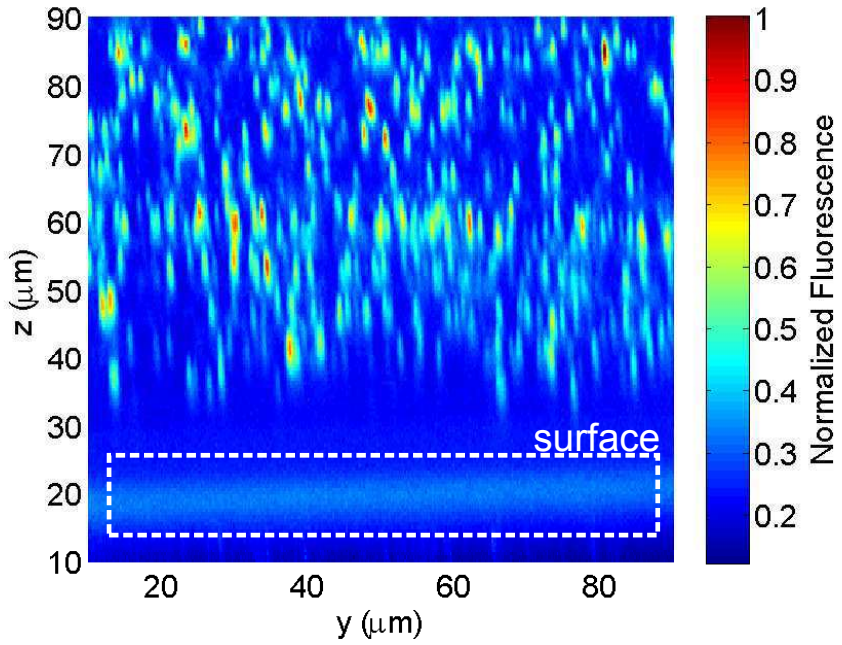

Figure 2.6: A $90\,\mu m \times 90\,\mu m$ depth scan into the diamond is performed along yz axis. Span from $15\,\mu m$ to $25\,\mu m$, a band of bright scattering from the surface can be observed. A huge number of fluorescence spot is observed across the diamond.

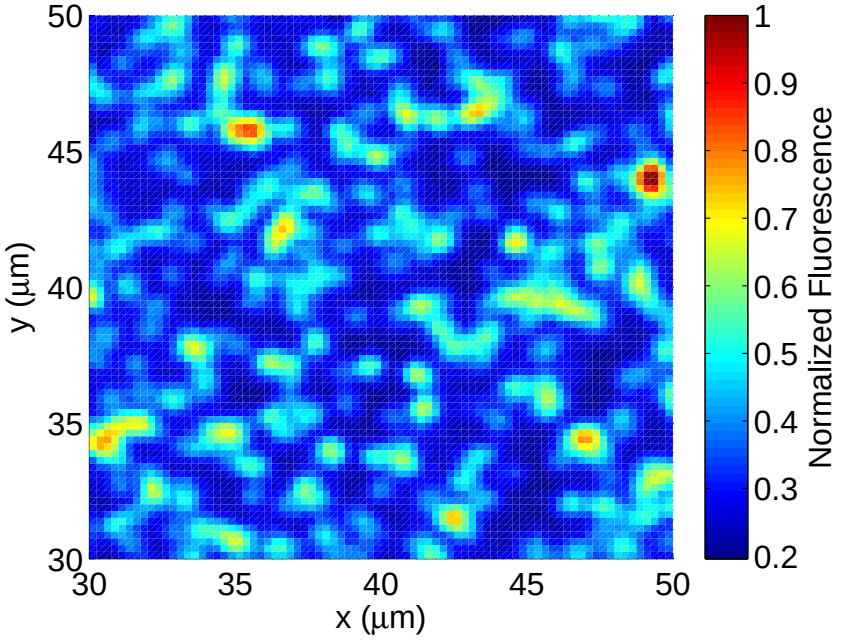

Figure 2.7: A $20\,\mu m \times 20\,\mu m$ lateral scan in the diamond is performed along xy axis. At this resolution individual bright spot can be observed and zoomed for further study.

scan (xy plane) in step of $0.1\,\mu m$ and fitting it to a Gaussian function as the following

$$\psi(x) = a\exp(\frac{-2(x-c)^2}{2w_0^2}) + b \tag{2.5}$$

where a is scaling factor, c is center of the fluorescence spot, w_0 is the waist size, b is background contribution. The lateral scan and its Gaussian fit to both x and y axis of the scan is shown in Figure 2.8. We obtain a waist size of $w_0 = 0.32 \pm 0.01\,\mu m$ for both x and y axis, indicating a good overlap of the excitation and collection mode. The agreement of measured waist ($w_0 = 0.32 \pm 0.01\,\mu m$) to the estimated waist ($w_0 = 0.326\,\mu m$) shows that alignment of the confocal microscope is optimum.

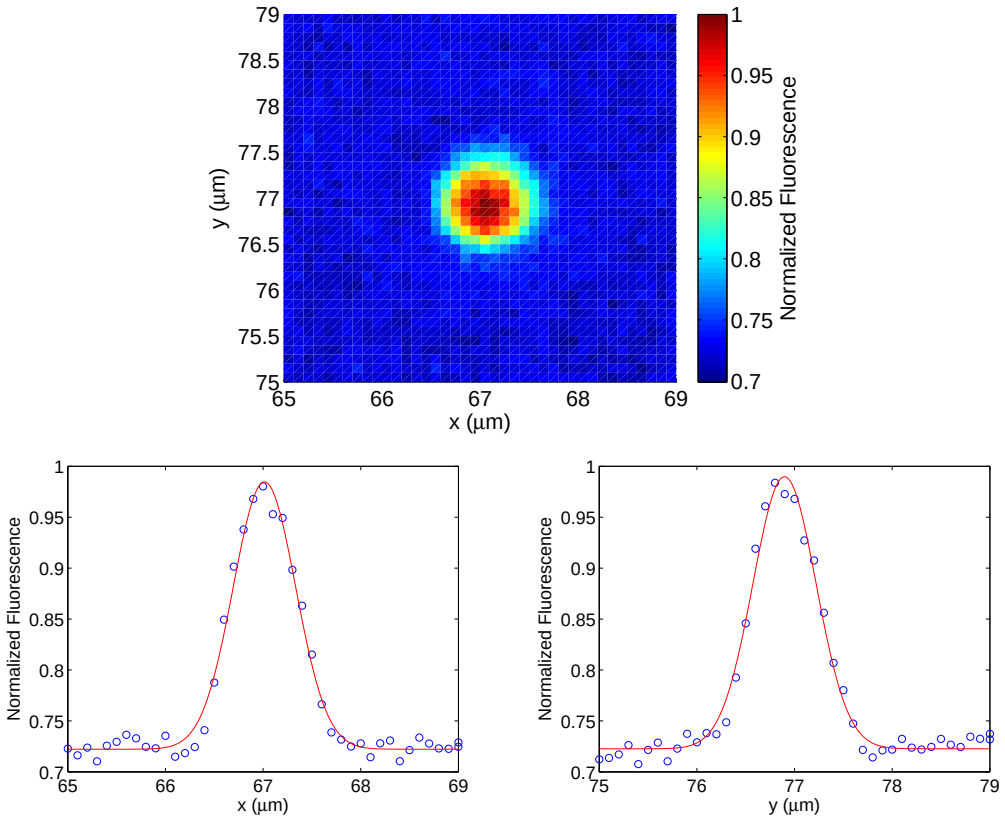

Figure 2.8: A lateral scan (xy) in step of $0.1\,\mu m$ of a fluorescence spot. Both scans are fitted to a Gaussian function (2.5) to extract the characteristic waist size. The waist sizes are same in both axis with $w_0 = 0.32 \pm 0.01\,\mu m$.

2.2.2 Power dependence

To select a suitable excitation power, we measure fluorescence count as a function of excitation power. The result is shown in Figure 2.9 and is fitted to function as the following

$$F = \frac{F_0 P}{P_{sat} + P} \tag{2.6}$$

where F is fluorescence count, F_0 is apparent fluorescence count, P is power, P_{sat} is saturation power. Fluorescence of the NV center clearly shows saturation behavior with P_{sat}=5.35 mW. The background fluorescence however increases linearly with power.

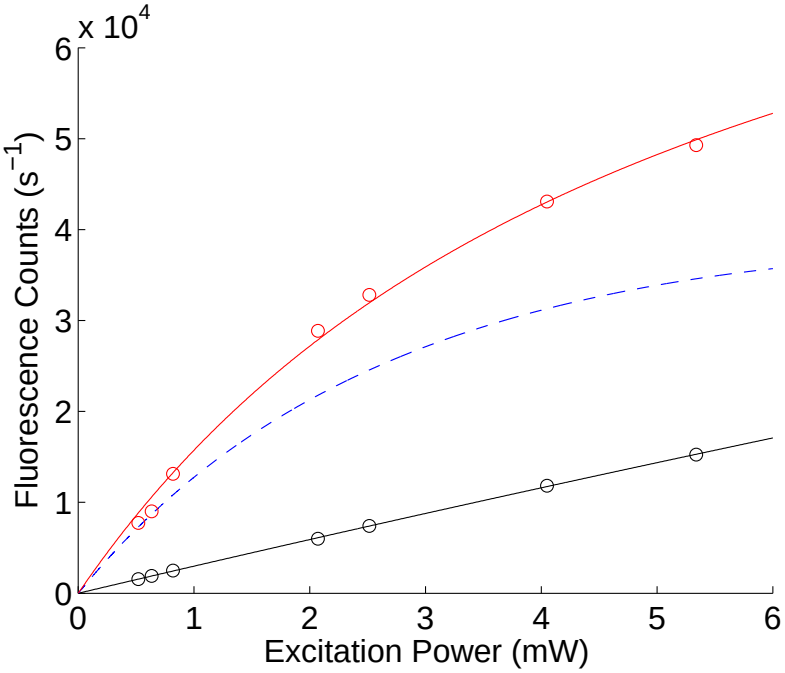

Figure 2.9: Fluorescence count as a function of excitation power for a NV center (Red) and background (Black). The data is fitted (Solid lines) to Equation 2.6. A subtract is plotted in blue dotted line.

2.3 Conclusion

We have built a confocal microscope that is capable of observing diffraction limited fluorescence from NV center in diamond. The characteristic waist size of the fluorescence agrees with our estimation, showing that the alignment of the confocal microscope is close to optimum. Fo-

cusing of the confocal microscope is also characterized by measuring dependence of fluorescence count on excitation power in which we obtained a saturation power of P_{sat}=5.34 mW.

Chapter 3

Spectroscopy of NV center

In this chapter, spectral properties of the detected fluorescence is studied. We want to confirm that the observed fluorescence comes from NV center, instead of other color centers that may present in a diamond. At room temperature, zero phonon line of NV center at 637 nm is clearly identifiable in addition to its characteristic vibrationally broadened spectrum that stretches from 630 nm to 750 nm.[6, 27] A home built grating spectrometer is used to measure spectrum of the fluorescence.

3.1 Setup: Grating spectrometer

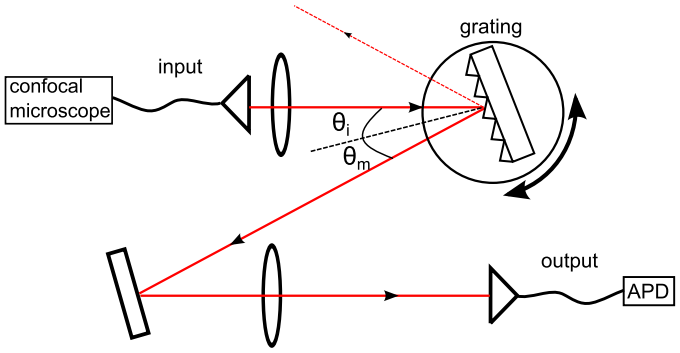

Figure 3.1: Schematic of the spectrometer used in this setup. A rotational motor is used to drive the movement of the diffraction grating.

In this experiment, we use a simple grating spectrometer as shown in Figure 3.1. For a diffraction grating, the zeroth order light obeys the law of reflection having $\theta_r = \theta_i$, while higher

m^{th} order reflections are governed by grating equation as the following

$$\frac{m\lambda}{d} = sin\theta_m - sin\theta_i \tag{3.1}$$

where m is order of diffraction, λ is wavelength of incident light, d is distance between grating grooves, θ_m is angle of reflection of m^{th} mode and θ_i is angle of incidence. We have used a diffraction grating with d=833 nm.

The spectrometer has to be calibrated to allow conversion from measured incident angle to detected fluorescence wavelength. The topology used in our calibration is chosen such that when θ_i=0, the first order reflection of the reference laser (HeNe, λ=632.8 nm) is detected, i.e. $m = 1$, $\lambda = 632.8\,\text{nm}$, $\theta_i = 0$ resulting in $\theta_1 = 49.43°$. This gives angular displacement between the signal and mirror of $\theta_i + \theta_1 = 49.43°$ in case of $\theta_i \neq 0$. With linear approximation, it is then possible to express the wavelength as a function of incident angle, given by

$$\lambda = 1.514 \times 10^{-6} cos(\theta_i + 1.14) \tag{3.2}$$

The resolution of the spectrometer is determined by the distance between grating grooves and numerical aperture of the collection optics. We measured resolution of 0.4 nm by determining the transmission bandwidth of the spectrometer given by a HeNe laser which linewidth is much smaller than expected resolution. The overall transmission of the spectrometer is measured to be 33.9%.

3.2 Results

Fluorescence signal obtained from the confocal microscope is sent to the spectrometer. Spectra for a fluorescent spot and background obtained with scanning step of approximately 0.122 nm, integration time per point of 30 s are shown in Figure 3.2. The 612 nm peak that is common to both spectra comes from second order Raman scattering of diamond crystalline.[28]

Fluorescence spectrum of the spot in the region from 630 nm to 750 nm, has a signal that resembles the vibrationally broadened side band of a NV center.

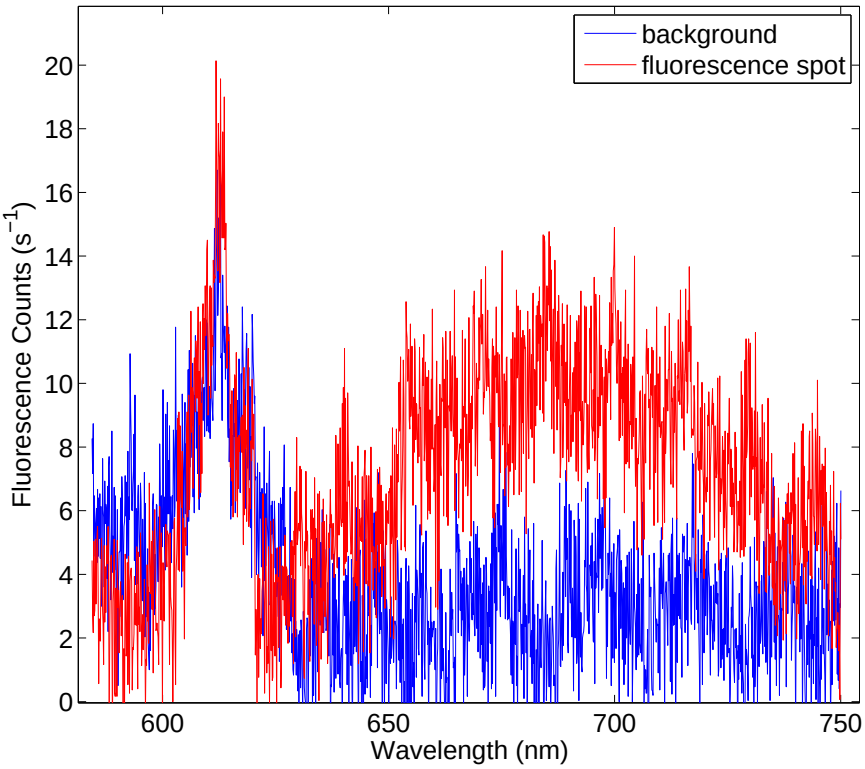

Figure 3.2: Fluorescence spectrum for a NV center (red) with a reference spectrum from the background (blue). The signature vibrationally broadened spectrum of a NV in regime of 630 nm to 750 nm is observed. The peak at 612 nm corresponds to second order Raman scattering of diamond crystalline.

However, the signature zero phonon line at 637 nm could not be resolved due to huge background noise. The background noise has an oscillation timescale of an hour. We suspect that this noise is related to power fluctuation of the excitation laser. Hence, the effect from power fluctuation is minimized by saturating the NV center, obtaining a spectrum as shown in Figure 3.3. In this spectrum, the zero phonon line at 637 nm is seen together with signature vibrationally broadened spectrum of NV center. The slight offset from 637 nm comes from error in approximation taken for spectrometer calibration.

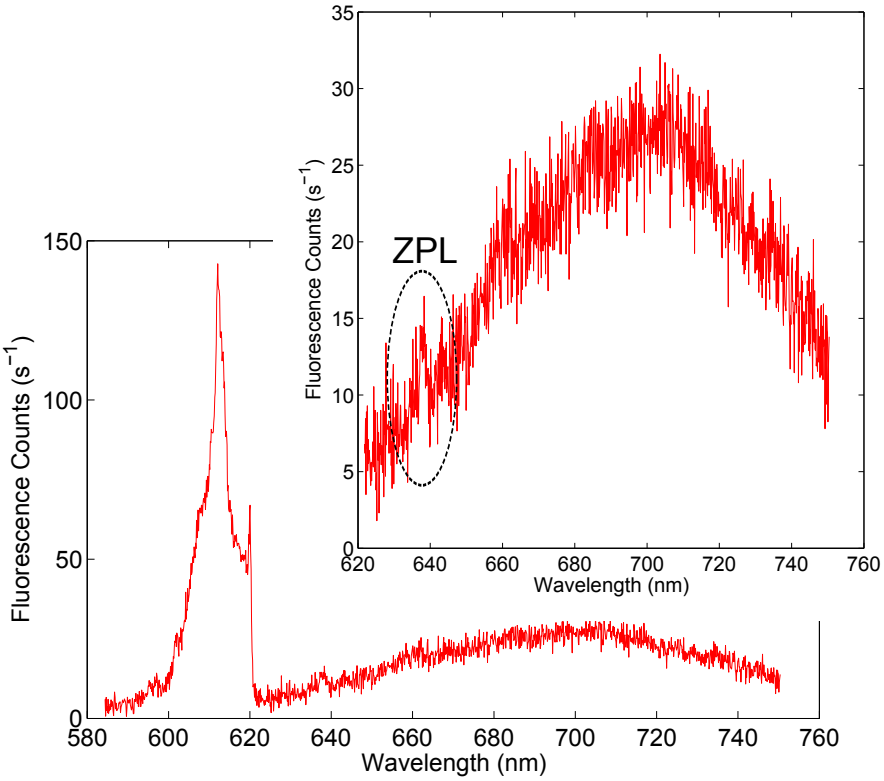

Figure 3.3: Fluorescence spectrum for a NV center with excitation power at saturation level to neglect the effect of power fluctuation. Zero phonon line (ZPL) at 637 nm and signature vibrationally broadened spectrum of NV center is observed. The peak at 612 nm corresponds to second order Raman scattering of diamond crystalline.

3.3 Conclusion

Spectrum of the fluorescence signal is measured with a grating spectrometer. We observed the signature vibrationally broadened spectrum of NV center that stretches across 630 nm to 750 nm. However, the zero phonon line emission of NV center at 637 nm is only observed with the use of excitation power above saturation level due power fluctuation in the system.

Chapter 4

NV center as single photon emitter

We wish to confirm that single NV center is observed by our confocal microscope. As it has been shown that NV center is single photon emitter[28], we verify our setup by performing Hanbury Brown Twiss (HBT) measurement to show photon antibunching effect of NV center.

4.1 Setup: Hanbury Brown and Twiss (HBT) interferometer

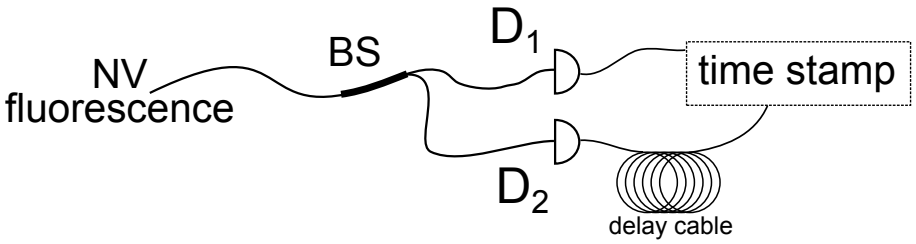

Figure 4.1: Schematic of a HBT interferometer. The fluorescence signal is passed through a beam splitter (BS) to be detected by two detectors (D_1, D_2) where each detected event is recorded by a time stamp unit.

To show the effect of photon antibunching, a HBT setup is used to measure second order intensity correlation function which is

$$g^{(2)}(\tau) = \frac{< I_1(t) I_2(t+\tau) >}{< I_1(t) >< I_2(t) >} \tag{4.1}$$

where τ is time delay between the detected events in D_1 and D_2, $I_1(t)$ is intensity at D_1 at time t, $I_2(t)$ is intensity at D_2 at time t, $< I_1(t) I_2(t+\tau) >$ is joint detected intensities by the

two detectors, while $< I_1(t) >< I_2(t) >$ is the normalization factor. In our case, the $g^{(2)}(\tau)$ is reconstructed by measuring the rates photodetection events in D_1 and D_2 that is proportional to fluorescence intensity.

The fluorescence signal obtained from confocal microscope is sent to a HBT setup shown in Figure 4.1. The $g^{(2)}(\tau)$ is measured by sending the signal to a beam splitter to be detected by two avalanche photodetectors (APD). The detection time in both APDs is recorded with a time stamp unit. Owing to the dead time effect of the time stamp (125 ns), a delay of 400 ns is introduced in the second channel such that occurrence of two events at the same time could still be detected. The data of the time stamp is processed by binning into time per bin of $t_{bin} = 1$ ns. The obtained count rates are used to compute $g^{(2)}(\tau)$ function. Explicitly, it is expressed as

$$g^{(2)}(\tau) = \frac{< N_1(t)N_2(t+\tau) >}{r_1 r_2 t_{bin} T} \tag{4.2}$$

where $< N_1(t)N_2(t+\tau) >$ is joint detected events (proportional to intensity), r_1 and r_2 is rate of detected events in D_1 and D_2, t_{bin} is time per bin, T is total measurement time. Ideally at $\tau = 0$ for a single quantum emitter, $g^{(2)}(0) = 0$ while classical sources would have $g^{(2)}(0) \geq 1$. However as $g^{(2)}(0) = 1/2$ would indicate a two photon state, it is sufficient to show single photon emission with $g^{(2)}(0) < 1/2$.

4.2 Results

Measured result of $g^{(2)}(\tau)$ is shown in Figure 4.2. We obtain $g^{(2)}(0) = 0.74 \pm 0.05$ which does not reach the expected value of 0 nor 0.5. The measurement is yet to be improved as there is two limiting factor to be solved in the near future. First, filtering has to be improved to remove the background contribution such that the collected signal is solely from the NV fluorescence. Moreover, the piezoelectric positioning of the diamond sample without active locking mechanism may be insufficient for long measurements. This might lead to displacement of NV center in and out of focus during the measurement. In this light, we intend to design a script to actively

correct the position of NV center by using detected counts as feedback.

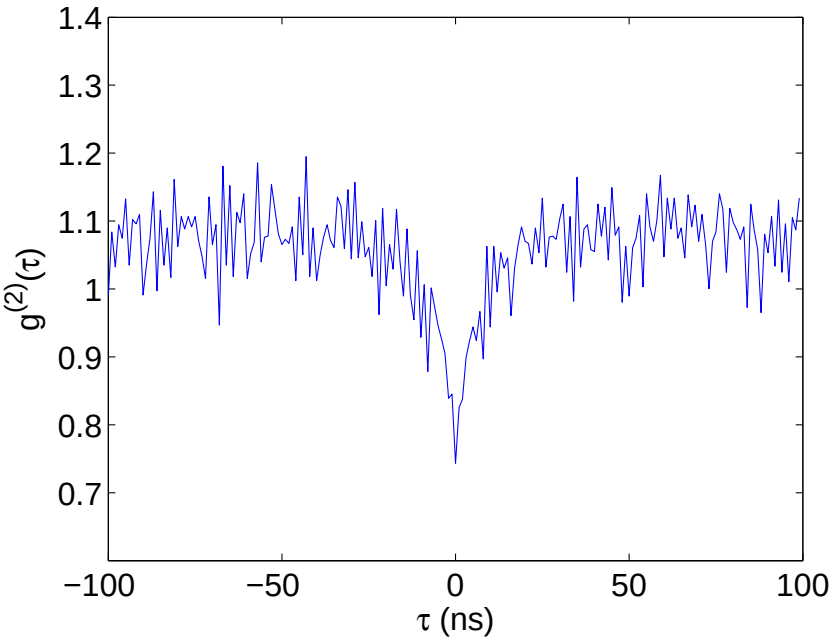

Figure 4.2: Measured second order correlation function $g^{(2)}(\tau)$ of a single NV center over integration time of $T = 24h$. $g^{(2)}(0) = 0.74 \pm 0.05$ is obtained.

4.3 Conclusion

Second order correlation intensity function $g^{(2)}(\tau)$ of the NV fluorescence is measured to verify observation of single NV center. We obtain $g^{(2)}(0) = 0.74 \pm 0.05$ which does not lead to expected result of photon antibunching. However, observation of a dip ($g^{(2)}(0) < 1$) clearly shows a non-classical light source. Nevertheless, further improvement is required for a conclusive result.

Chapter 5

Conclusion

We have built a confocal microscope that is capable of observing diffraction limited fluorescence from NV center in diamond. Characteristic waist size of the fluorescence agrees with our estimation, showing that alignment of the confocal microscope is close to optimum. Focusing of the confocal microscope is also characterized by measuring dependence of fluorescence count on excitation power. We obtained a saturation power of P_{sat}=5.34 mW.

Furthermore, spectrum of the fluorescence signal is measured with a grating spectrometer. We observed signature vibrationally broadened spectrum of NV center that stretches across 630nm to 750nm. However, zero phonon line emission of NV center at 637nm is only observed with the use of excitation power above saturation level due power fluctuation in the system.

Second order correlation intensity function $g^{(2)}(\tau)$ of the NV fluorescence is measured to verify observation of single NV center. We obtain $g^{(2)}(0) = 0.74 \pm 0.05$ which does not lead to expected result of photon antibunching. However, observation of a dip ($g^{(2)}(0) < 1$) clearly shows a non-classical light source. Nevertheless, further improvement is required for a conclusive result.

In the near future, we wish to implement a script to actively reposition the piezoelectric stage to ensure NV center stays within the focus even in long measurement. The $g^{(2)}(\tau)$ of NV center will then be measured again by using a long pass filter to remove the contribution of second

order Raman scattering at 612 nm. From then, we proceed the setup to measure magnetic field, starting from building source of 2.88 GHz to drive the ground electronic spin state.

Bibliography

[1] D. Budker and M. V. Romalis, "Optical magnetometry," *Nature Physics*, vol. 3, no. 4, p. 11, 2006.

[2] J. Aguayo, S. Blackband, and J. Schoeniger, "Nuclear magnetic resonance imaging of a single cell," *Nature*, vol. 322, pp. 190–191, 1986.

[3] L. Ciobanu, D. Seeber, and C. Pennington, "3D MR microscopy with resolution 3.7μm by 3.3μm by 3.3μm," *Journal of Magnetic Resonance*, vol. 158, no. 12, pp. 178 – 182, 2002.

[4] D. Rugar, R. Budakian, H. J. Mamin, and B. W. Chui, "Single spin detection by magnetic resonance force microscopy.," *Nature*, vol. 430, pp. 329–32, July 2004.

[5] P. Glover and S. P. Mansfield, "Limits to magnetic resonance microscopy," *Reports on Progress in Physics*, vol. 65, pp. 1489–1511, Oct. 2002.

[6] a. Gruber, A. Dräbenstedt, C. Tietz, and L. Fleury, "Scanning confocal optical microscopy and magnetic resonance on single defect centers," *Science*, vol. 276, pp. 2012–2014, June 1997.

[7] J. M. Taylor, P. Cappellaro, L. Childress, L. Jiang, D. Budker, P. R. Hemmer, A. Yacoby, R. Walsworth, and M. D. Lukin, "High-sensitivity diamond magnetometer with nanoscale resolution," *Nature Physics*, vol. 4, no. 10, p. 29, 2008.

[8] C. L. Degen, "Scanning magnetic field microscope with a diamond single-spin sensor," *Applied Physics Letters*, vol. 92, no. 24, p. 4, 2008.

[9] G. Balasubramanian, I. Y. Chan, R. Kolesov, M. Al-Hmoud, J. Tisler, C. Shin, C. Kim, A. Wojcik, P. R. Hemmer, A. Krueger, T. Hanke, A. Leitenstorfer, R. Bratschitsch, F. Jelezko, and J. Wrachtrup, "Nanoscale imaging magnetometry with diamond spins under ambient conditions.," *Nature*, vol. 455, pp. 648–51, Oct. 2008.

[10] "Nanoscale magnetic sensing with an individual electronic spin in diamond.," *Nature*, vol. 455, pp. 644–647, Oct. 2008.

[11] "Ultralong spin coherence time in isotopically engineered diamond.," *Nature materials*, vol. 8, pp. 383–7, May 2009.

[12] P. C. Maurer, J. R. Maze, P. L. Stanwix, L. Jiang, a. V. Gorshkov, a. a. Zibrov, B. Harke, J. S. Hodges, a. S. Zibrov, a. Yacoby, D. Twitchen, S. W. Hell, R. L. Walsworth, and M. D. Lukin, "Far-field optical imaging and manipulation of individual spins with nanoscale resolution," *Nature Physics*, vol. 6, pp. 912–918, Sept. 2010.

[13] B. R. Smith, D. W. Inglis, B. Sandnes, J. R. Rabeau, A. V. Zvyagin, D. Gruber, C. J. Noble, R. Vogel, E. Osawa, and T. Plakhotnik, "Five-nanometer diamond with luminescent nitrogen-vacancy defect centers.," *Small Weinheim an der Bergstrasse Germany*, vol. 5, no. 14, pp. 1649–1653, 2009.

[14] C. Bradac, T. Gaebel, N. Naidoo, J. R. Rabeau, and A. S. Barnard, "Prediction and measurement of the size-dependent stability of fluorescence in diamond over the entire nanoscale.," *Nano Letters*, vol. 9, no. 10, pp. 3555–3564, 2009.

[15] T. M. Babinec, B. J. M. Hausmann, M. Khan, Y. Zhang, J. R. Maze, P. R. Hemmer, and M. Loncar, "A diamond nanowire single-photon source.," *Nature nanotechnology*, vol. 5, pp. 195–9, Mar. 2010.

[16] S. Steinert, F. Dolde, P. Neumann, A. Aird, B. Naydenov, G. Balasubramanian, F. Jelezko, and J. Wrachtrup, "High sensitivity magnetic imaging using an array of spins in diamond," *Review of Scientific Instruments*, vol. 81, no. 4, p. 043705, 2010.

[17] V. M. Acosta, E. Bauch, A. Jarmola, L. J. Zipp, M. P. Ledbetter, and D. Budker, "Broadband magnetometry by infrared-absorption detection of nitrogen-vacancy ensembles in diamond," *Applied Physics Letters*, vol. 97, no. 17, p. 174104, 2010.

[18] B. J. Maertz, A. P. Wijnheijmer, G. D. Fuchs, M. E. Nowakowski, and D. D. Awschalom, "Vector magnetic field microscopy using nitrogen vacancy centers in diamond," *Applied Physics Letters*, vol. 96, no. 9, p. 092504, 2010.

[19] a. Lenef and S. Rand, "Electronic structure of the NV center in diamond: theory," *Physical Review B*, vol. 53, no. 20, pp. 13441–13455, 1996.

[20] M. V.H., A.-R. Y.M., and M. J.P.D., "Fine structure of excited 3e state in nitrogen-vacancy centre of diamond," *Journal of Luminescence*, vol. 81, no. 4, pp. 237–247, 1999.

[21] T. Gaebel, M. Domhan, C. Wittmann, I. Popa, F. Jelezko, J. Rabeau, A. Greentree, S. Prawer, E. Trajkov, P. R. Hemmer, and et al., "Photochromism in single nitrogen-vacancy defect in diamond," *Applied Physics B*, vol. 82, no. 2, p. 11, 2005.

[22] Y. Mita, "Change of absorption spectra in type- b diamond with heavy neutron irradiation," *Phys. Rev. B*, vol. 53, pp. 11360–11364, May 1996.

[23] J. P. Goss, R. Jones, P. R. Briddon, G. Davies, A. T. Collins, A. Mainwood, J. A. van Wyk, J. M. Baker, M. E. Newton, A. M. Stoneham, and S. C. Lawson, "Comment on "electronic structure of the n-v center in diamond: theory"," *Phys. Rev. B*, vol. 56, pp. 16031–16032, Dec 1997.

[24] F. Jelezko, C. Tietz, A. Gruber, I. Popa, A. Nizovtsev, S. Kilin, and J. Wrachtrup, "Spectroscopy of single n-v centers in diamond," *Single Molecules*, vol. 2, no. 4, pp. 255–260, 2001.

[25] E. Hecht, *Optics*. Addison-Wesley, 2002.

[26] C. Davis, *Lasers and Electro-Optics: Fundamentals and Engineering*. Cambridge University Press, 1996.

[27] *The Properties of Natural and Synthetic Diamond*. edited by J. E. Field (Academic Press, London, 1992).

[28] C. Kurtsiefer, S. Mayer, P. Zarda, and H. Weinfurter, "Stable solid-state source of single photons," *Physical Review Letters*, vol. 85, no. 2, pp. 290–3, 2000.